Applied Catalysis B: Environmental 89 (2009) 87–96

Contents lists available at ScienceDirect

Applied Catalysis B: Environmental

journal homepage: www.elsevier.com/locate/apcatb

Preparation, characterization, and catalytic properties of $NdSrCu_{1-x}Co_xO_{4-\delta}$ and $Sm_{1.8}Ce_{0.2}Cu_{1-x}Co_xO_{4+\delta}$ ($x = 0$, 0.2 and 0.4) for methane combustion

Jiguang Deng [a], Lei Zhang [a], Hongxing Dai [a,*], Hong He [a], Chak Tong Au [b]

[a] Laboratory of Catalysis Chemistry and Nanoscience, Department of Chemistry and Chemical Engineering, College of Environmental and Energy Engineering, Beijing University of Technology, Ping-Le-Yuan 100, Chao Yang District, Beijing 100124, PR China
[b] Department of Chemistry, Center for Surface Analysis and Research, Hong Kong Baptist University, Kowloon Tong, Hong Kong, PR China

ARTICLE INFO

Article history:
Received 20 July 2008
Received in revised form 13 October 2008
Accepted 11 November 2008
Available online 18 November 2008

Keywords:
Perovskite-like oxide catalysts
$NdSrCu_{1-x}Co_xO_{4-\delta}$
$Sm_{1.8}Ce_{0.2}Cu_{1-x}Co_xO_{4+\delta}$
Methane combustion
Oxygen nonstoichiometry

ABSTRACT

Single-phase perovskite-like oxides $NdSrCu_{1-x}Co_xO_{4-\delta}$ and $Sm_{1.8}Ce_{0.2}Cu_{1-x}Co_xO_{4+\delta}$ ($x = 0$, 0.2, and 0.4) were prepared using the citric acid complexing method coupled with ultrasonic treatment. We characterized the materials by a number of analytical techniques. It was found that the $NdSrCu_{1-x}Co_xO_{4-\delta}$ and $Sm_{1.8}Ce_{0.2}Cu_{1-x}Co_xO_{4+\delta}$ catalysts possess *T* and *T'* crystal structures, respectively. There are Cu^{3+}/Cu^{2+} ions and oxygen vacancies in the former and Cu^{2+}/Cu^{+} ions and extra (over-stoichiometric) oxygen in the latter. We examined the catalytic activity of the materials for methane combustion. Methane conversion increased with a rise in the amount of nonstoichiometric oxygen over the two series of catalysts. It is concluded that oxygen nonstoichiometry and Cu^{3+}/Cu^{2+} or Cu^{2+}/Cu^{+} redox couples facilitate the oxidation of methane over the $NdSrCu_{1-x}Co_xO_{4-\delta}$ and $Sm_{1.8}Ce_{0.2}Cu_{1-x}Co_xO_{4+\delta}$ catalysts.

1. Introduction

The combustion of methane in air at high temperatures (above 1100 °C) would inevitably produce nitrogen oxides (NO_x). It is hence desirable to lower the combustion temperature by catalytic means. Due to their high activity and thermal stability, perovskite-type oxides (ABO_3) have been tested for the complete oxidation of methane [1–15]. Many studies showed that their catalytic activity is mainly dependent on the nature of the B component [3,4,13,16–21]. The partial substitution of the A-site [3,4,13,18,19], B-site [20,21] or both A- and B-site cations [22,23] by other ones can result in a significant change in catalytic activity. The outcome of such a kind of substitution could be either positive or negative.

To the best of our knowledge, there are only a few publications involving the catalytic properties of La_2NiO_4 and $La_{1.8}M_{0.2}CuO_4$ (M = Pr, Sm, Tb) for methane combustion [6,24–26]. Unfortunately, these authors did not give a clear relationship between the catalyst composition/structure and catalytic performance for the addressed reaction. There is no literature on the comparative investigation of catalytic properties of perovskite-like mixed oxides (A_2BO_4) with large amounts of oxygen vacancies and oxygen excess for methane combustion. Similar to the case of ABO_3, it is possible to have the A- or B-site ions of A_2BO_4 changed or partially substituted. Mizuno et al. [27] showed that the valence of copper in La_2CuO_4 could be controlled by having La partially substituted with Sr or Ce as well as having Cu partially substituted with Al or Zr, and the compound became oxygen-rich upon Al^{3+}, Zr^{4+}, and Ce^{4+} substitution and oxygen-deficient upon Sr^{2+} substitution. They found that the activity of CO and NO interaction over the catalysts could be related to the oxidation states of copper. Working on the simultaneous removal of CO, NO, and C_3H_6 over $La_2Cu_{1-x}Pd_xO_4$, Guilhaume et al. [28] observed that the activity of $La_2Cu_{0.8}Pd_{0.2}O_4$ was comparable to that of 1.13 wt% Pt–0.19 wt% $Rh/CeO_2–Al_2O_3$ under similar conditions. More recently, several research groups have investigated the catalysis of other perovskite-like mixed oxides, such as the catalytic combustion of C_3H_6 over $La_{2-x}Sr_xCuO_4S_y$ [29], the oxidation of CO and C_3H_8 over $La_{2-x}Sr_xCoO_{4\pm\lambda}$ [30], the decomposition of NO over $La_{2-x}Th_xCuO_4$ [31], the simultaneous removal of NO_x and diesel soot particulates over $La_{2-x}Na_xCuO_4$ [32], and the reduction of NO by CO over $La_{2-x}Sr_xCuO_4$ [33]. According to the authors, the A_2BO_4 compounds are thermally stable and the good catalytic activities may be related to the structural defects and redox behaviors (i.e. $B^{n+} \Leftrightarrow B^{(n+1)+}$) of A_2BO_4.

Considering the difference in structural defect of Sr- and Ce-doped A_2BO_4 compounds, along with the necessity in understanding the inherent reason for their discrepancy in activity, we herein report the preparation, characterization, and catalytic performance of $NdSrCu_{1-x}Co_xO_{4-\delta}$ and $Sm_{1.8}Ce_{0.2}Cu_{1-x}Co_xO_{4+\delta}$ ($x = 0$, 0.2, 0.4) that possess large amounts of oxygen vacancies and

* Corresponding author. Tel.: +86 10 6739 6588; fax: +86 10 6739 1983.
E-mail address: hxdai@bjut.edu.cn (H. Dai).

0926-3373/$ – see front matter © 2008 Elsevier B.V. All rights reserved.
doi:10.1016/j.apcatb.2008.11.015

oxygen excess, respectively, for the combustion of methane. It is shown that good catalytic performance can be achieved by manipulating the nature of oxygen nonstoichiometry and the redox ability of copper ion couples.

2. Experimental

2.1. Catalyst preparation

The $NdSrCu_{1-x}Co_xO_{4-\delta}$ and $Sm_{1.8}Ce_{0.2}Cu_{1-x}Co_xO_{4+\delta}$ (x = 0, 0.2, 0.4) catalysts were prepared by the citric acid complexing method that coupled with ultrasonic treatment. The application of ultrasonic treatment during the citric acid-complexing process is beneficial for the formation of highly dispersed metal complexes and hence for the generation of catalysts with relatively high-surface areas. Stoichiometric amounts of high-purity (Aldrich, >99%) nitrates of neodymium, strontium, copper, and cobalt for $NdSrCu_{1-x}Co_xO_{4-\delta}$ (or nitrates of samarium, cerium, copper, and cobalt for $Sm_{1.8}Ce_{0.2}Cu_{1-x}Co_xO_{4+\delta}$) were dissolved in deionized water. Under ultrasonic treatment, an excess amount of citric acid (metal/citric acid molar ratio = 1/1.5) was added. Under constant stirring, the solution was evaporated at 80 °C until a viscous gel was formed. The gel was transferred to a muffle furnace and it was abruptly converted to fine powders at around 400 °C. After thorough grinding, the powders were calcined in air at 950 °C for 10 h. The as-obtained powders were pressed, crushed, and sieved to 40–60 meshes for subsequent uses.

2.2. Chemical analysis of Cu ion oxidation states

The contents of Cu^{3+} in $NdSrCu_{1-x}Co_xO_{4-\delta}$ and Cu^+ ions in $Sm_{1.8}Ce_{0.2}Cu_{1-x}Co_xO_{4+\delta}$ were determined using a rather popular method of titrimetric analysis based on the oxidation of ferrous ions ($Cu^{3+} + Fe^{2+} \rightarrow Cu^{2+} + Fe^{3+}$) or the reduction of ferric ions ($Cu^+ + Fe^{3+} \rightarrow Cu^{2+} + Fe^{2+}$) [34]. The sample (0.2 g) was dissolved in 2.6 M H_3PO_4 solution containing standard 0.1 M Fe^{2+} (Mohr's salt, $(NH_4)_2Fe(SO_4)_2{\cdot}6H_2O$) solution under N_2 atmosphere. The Fe^{2+} that remained after the $Cu^{3+} + Fe^{2+} \rightarrow Cu^{2+} + Fe^{3+}$ reaction was titrated against standard 0.017 M potassium dichromate solution. For the determination of Cu^+ content, 0.2 g of the sample was dissolved in 2.6 M H_3PO_4 solution containing standard 0.1 M Fe^{3+}. The Fe^{3+} ions were reduced to Fe^{2+} according to the $Cu^+ + Fe^{3+} \rightarrow Cu^{2+} + Fe^{2+}$ reaction and the amount of Fe^{2+} ions formed was determined by titrating the solution against standard 0.017 M potassium dichromate solution with sodium 4-diphenylamine sulfonate being the indicator. The experimental errors for the determination of Cu^{3+} and Cu^+ contents according to the methods are estimated to be ±0.20%.

2.3. Catalyst characterization

The crystal structures of the catalysts were determined on an X-ray diffractometer (XRD, Bruker/AXS D8 Advance) with Cu Kα radiation (40 kV and 200 mA). The acquired patterns were referred to the JCPDS data for phase identification. Surface morphologies of the samples were measured using the scanning electron microscope (SEM, JEOL JSM 6500F) operated at an accelerating voltage of 30 kV. X-ray photoelectron spectroscopy (XPS) technique (VG CLAM 4 MCD) was used to determine the Nd $3d_{5/2}$, Sr $3d_{5/2}$, Sm $3d_{5/2}$, Ce 3d, Cu $2p_{3/2}$, Co $2p_{3/2}$, and O 1s binding energies (BE) of surface species. The pass energy was 20 eV, giving a full width at half maximum of 1.2 eV for the Ag $3d_{5/2}$ line at a Mg Kα setting of 10 kV × 15 mA. Before XPS measurements, the samples were calcined in an O_2 flow of 20 mL/min at 800 °C for 1 h and then cooled to room temperature (RT), followed by helium (20 mL/min) purging for 1 h at RT. After the above treatment, the samples were mounted and transferred to the spectrometer in a transparent GLOVE BAG (Instruments for Research and Industry, USA) filled with helium to avoid exposure to air. Finally, the samples were outgassed in the preparation chamber (10^{-5} Torr) for 0.5 h and then introduced into the analysis chamber (3×10^{-9} Torr) for recording. The C 1s line at 284.6 eV of surface adventitious carbon was taken as a reference for BE calibration. The relative energy accuracy was ±0.5 eV for all the samples. The specific surface areas of the catalysts were determined by nitrogen adsorption–desorption isotherm measurements at −196 °C on a Micromeritics ASAP 2010 nitrogen adsorption apparatus. The samples were degassed at 200 °C for 2 h prior to measurements.

For the O_2-TPD (temperature-programmed desorption) studies, the sample (0.1–0.2 g) was placed in the middle of a quartz microreactor of 8-mm i.d. The outlet gases were analyzed on-line by mass spectrometry (Hiden HPR20). The heating rate was 10 °C/min and the temperature range was RT to 950 °C. Before an O_2-TPD experiment, the sample was calcined in pure O_2 (99.99%, flow rate = 20 mL/min) at 800 °C for 1 h, followed by cooling in oxygen to RT and helium purging (40 mL/min) for 4 h. The helium-purging step was aimed to remove all the gas-phase oxygen in the system. The amount of O_2 desorbed from the catalyst was quantified by calibrating the peak area against that of a standard O_2 pulse (50.0 μL).

Hydrogen temperature-programmed reduction (H_2-TPR) was carried out in a quartz fixed-bed micro-reactor (i.d. = 6 mm) in the RT–900 °C range. The sample (0.1–0.2 g) was treated in an oxygen flow (50 mL/min) at 500 °C for 1 h and then cooled down to RT in the same atmosphere. After being purged in a N_2 flow (50 mL/min) for 30 min, the treated sample was reduced in a flow of 5% H_2/Ar (50 mL/min) at a ramping rate of 10 °C/min. The effluent was monitored with a thermal conductivity detector. The thermal conductivity response was calibrated against the reduction of a known CuO powder sample (Aldrich, 99.995%).

2.4. Catalytic activity evaluation

The catalytic activities were evaluated with the sample secured in a continuous flow fixed-bed quartz microreactor (i.d. = 8 mm) at atmospheric pressure. The catalysts (0.1–0.3 g, 40–60 mesh) were well mixed with equal amount (by mass) of quartz sand (40–60 mesh). Before each run, the catalysts were activated in a stream of pure O_2 (40 mL/min) at 800 °C for 1 h (for the total removal of adsorbed impurities), then cooled to 200 °C. The molar feed composition was "0.5% CH_4 + 10% O_2 + balance N_2" at a space velocity of 10,000 h^{-1}. Under the same reaction conditions, we measured the activities of quartz sands and sol–gel-derived $LaCoO_3$. For the changes of space velocity and methane/O_2 molar ratio, we altered the amount of catalyst and mass flow of oxygen, respectively. The inlet and outlet gas compositions were analyzed on-line by gas chromatograph (GC–14C) with Porapak Q and 5A Molecular Sieve columns. Carbon balance was close to 99% in each run.

3. Results

3.1. XRD, BET, and chemical analysis studies

Fig. 1 shows the XRD patterns of $NdSrCu_{1-x}Co_xO_{4-\delta}$ and $Sm_{1.8}Ce_{0.2}Cu_{1-x}Co_xO_{4+\delta}$. All of the discernible diffraction peaks can be indexed as indicated in the figure. By referring to the JCPDS Database data (PDF nos. 38–1427, 39–1190, and 39–1390), one can realize that the two series of catalysts displayed single-phase tetragonal geometries, in which $NdSrCu_{1-x}Co_xO_{4-\delta}$ show T structure while $Sm_{1.8}Ce_{0.2}Cu_{1-x}Co_xO_{4+\delta}$ exhibit T' structure. Fig. 2 shows the schematic crystal structures of

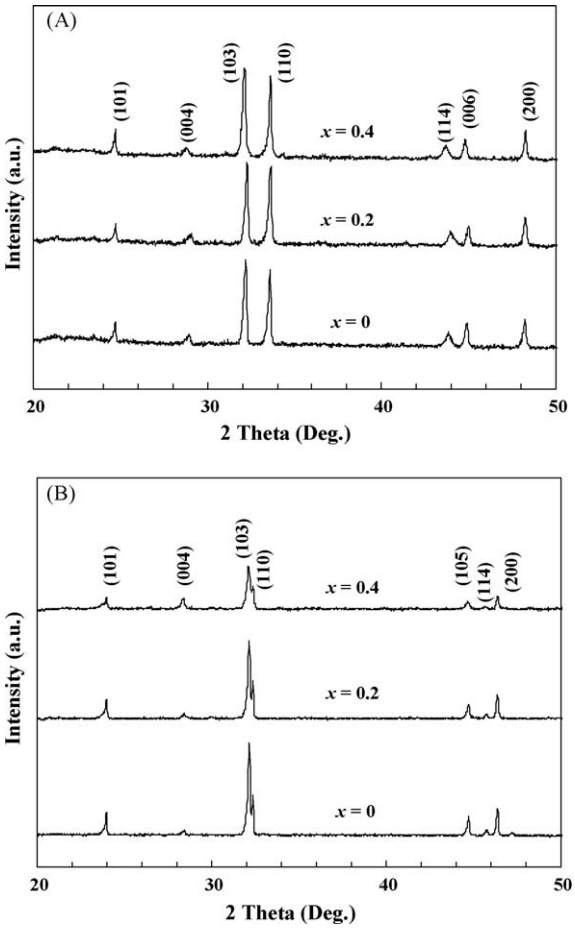

Fig. 1. XRD patterns of (A) $NdSrCu_{1-x}Co_xO_{4-\delta}$ and (B) $Sm_{1.8}Ce_{0.2}Cu_{1-x}Co_xO_{4+\delta}$.

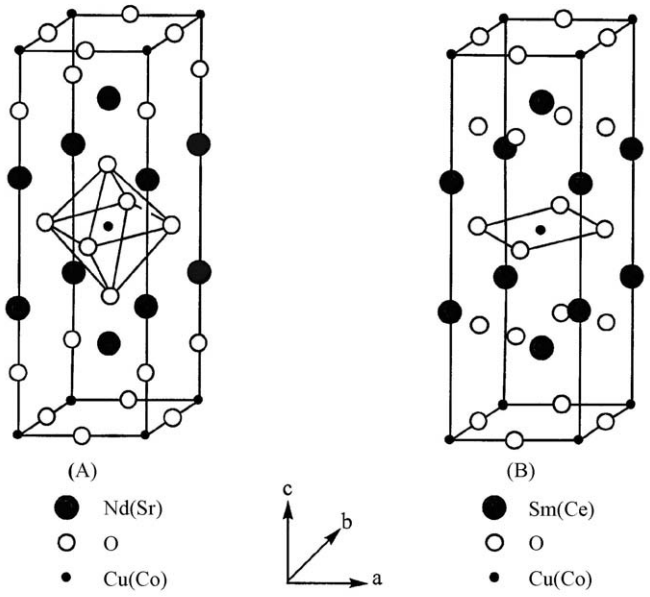

Fig. 2. Crystal structures of (A) $NdSrCu_{1-x}Co_xO_{4-\delta}$ (*T* structure) and (B) $Sm_{1.8}Ce_{0.2}Cu_{1-x}Co_xO_{4+\delta}$ (*T′* structure).

$NdSrCu_{1-x}Co_xO_{4-\delta}$ and $Sm_{1.8}Ce_{0.2}Cu_{1-x}Co_xO_{4+\delta}$. It can be seen that there are apical oxygen atoms in the *T* structure whereas in the *T′* structure the apical oxygen atoms are missing.

The crystal phases, compositions, and surface areas of $NdSrCu_{1-x}Co_xO_{4-\delta}$ and $Sm_{1.8}Ce_{0.2}Cu_{1-x}Co_xO_{4+\delta}$ are summarized in Table 1. Based on the results of Cu^{3+} or Cu^{+} titration as well as the assumption of electroneutrality, the δ values of the catalysts are estimated. Apparently, the $NdSrCu_{1-x}Co_xO_{4-\delta}$ catalysts belong to the category of reductive nonstoichiometry while the $Sm_{1.8}Ce_{0.2}Cu_{1-x}Co_xO_{4+\delta}$ catalysts oxidative nonstoichiometry [2]. With a rise in the extent of Co doping, the δ value of the former decreases and that of the latter increases. One can deduce that the substitution of Co for Cu at the B-sites lowers the amount of oxygen vacancies in $NdSrCu_{1-x}Co_xO_{4-\delta}$ but enhances the amount of over-stoichiometric oxygen in $Sm_{1.8}Ce_{0.2}Cu_{1-x}Co_xO_{4+\delta}$. In addition, the doping of Co gives rise to a change in the oxidation state of Cu ions of the two series of catalysts.

The surface areas of $NdSrCu_{1-x}Co_xO_{4-\delta}$ and $Sm_{1.8}Ce_{0.2}Cu_{1-x}Co_xO_{4+\delta}$ are within the 3.5–6.8 and 7.2–8.4 m^2/g ranges, respectively (Table 1). It is apparent that Co doping of the latter does not cause a significant change in surface area. In the case of $NdSrCu_{1-x}Co_xO_{4-\delta}$, surface area decreases from 6.8 to 3.5 m^2/g when the *x* value rises from 0 to 0.4. The $NdSrCu_{1-x}Co_xO_{4-\delta}$ and $Sm_{1.8}Ce_{0.2}Cu_{1-x}Co_xO_{4+\delta}$ microparticles display various morphologies (Fig. 3): (i) for the $NdSrCu_{1-x}Co_xO_{4-\delta}$ samples, there is a morphological evolution from macroporous woven-like to adobe-like architecture at elevated Co doping; and (ii) for the $Sm_{1.8}Ce_{0.2}Cu_{1-x}Co_xO_{4+\delta}$ samples, petal-like or porous morphologies are formed.

3.2. XPS studies

It is observed that there is no significant change in the position of the Nd $3d_{5/2}$ (BE = ca. 982 eV) and Sr $3d_{5/2}$ (BE = ca. 133 eV) XPS peaks of $NdSrCu_{1-x}Co_xO_{4-\delta}$, and in the position of the Sm $3d_{5/2}$ (BE = ca. 1082 eV) XPS peaks of $Sm_{1.8}Ce_{0.2}Cu_{1-x}Co_xO_{4+\delta}$ upon the variation of Co doping. Based on the corresponding BE, one can deduce that the oxidation state of Nd and Sr in $NdSrCu_{1-x}Co_xO_{4-\delta}$ and that of Sm in $Sm_{1.8}Ce_{0.2}Cu_{1-x}Co_xO_{4+\delta}$ are 3+, 2+, and 3+, respectively. As for the Ce 3d spectra of $Sm_{1.8}Ce_{0.2}Cu_{1-x}Co_xO_{4+\delta}$, there are two sets of three peaks at BE = 882.5, 889.4, and 898.7 eV and at BE = 900.6, 907.7, and 916.6 eV that can be ascribed to Ce $3d_{5/2}$ and Ce $3d_{3/2}$ signals, respectively. By referring to the Ce 3d

Table 1
Crystal phase, composition and surface area of catalysts.

Catalyst	Crystal phase[a]	Cu^{3+} or Cu^{+} conc.[b] (mol%)[c]	δ	Surface area (m^2/g)
$NdSrCuO_{4-\delta}$	*T*	40.5	0.30	6.8
$NdSrCu_{0.8}Co_{0.2}O_{4-\delta}$	*T*	34.1	0.26	5.4
$NdSrCu_{0.6}Co_{0.4}O_{4-\delta}$	*T*	29.7	0.21	3.5
$Sm_{1.8}Ce_{0.2}CuO_{4+\delta}$	*T′*	11.1	0.05	7.2
$Sm_{1.8}Ce_{0.2}Cu_{0.8}Co_{0.2}O_{4+\delta}$	*T′*	23.8	0.10	7.5
$Sm_{1.8}Ce_{0.2}Cu_{0.6}Co_{0.4}O_{4+\delta}$	*T′*	37.6	0.19	8.4

[a] *T* and *T′* denotes tetragonal structure. The only difference between *T* and *T′* structures is that there are no apical oxygen atoms in the *T′* structure.
[b] Assuming that there are only Cu^{3+} and Cu^{2+} ions in $NdSrCu_{1-x}Co_xO_{4-\delta}$ catalysts or Cu^{+} and Cu^{2+} ions in $Sm_{1.8}Ce_{0.2}Cu_{1-x}Co_xO_{4+\delta}$ catalysts.
[c] Data uncertainty: ±0.2.

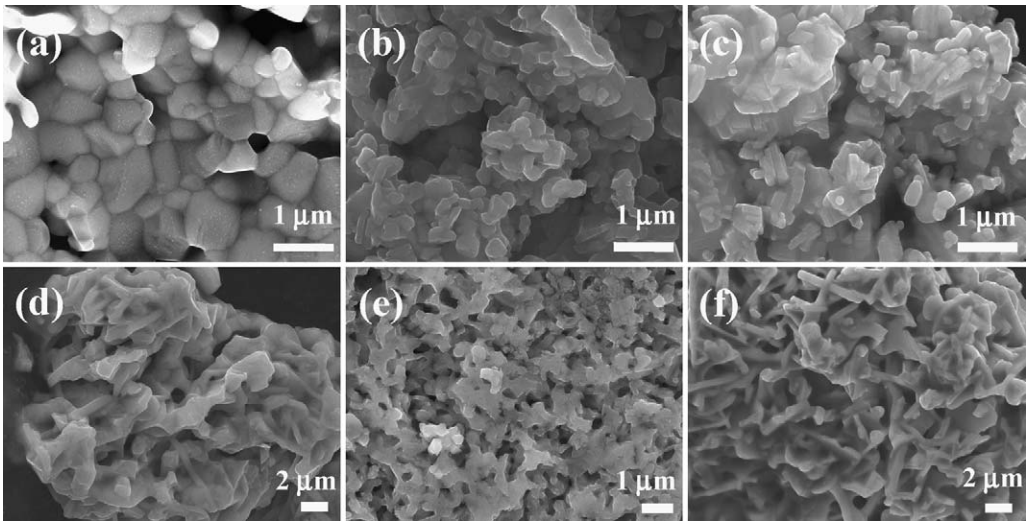

Fig. 3. SEM images of (a–c) $NdSrCu_{1-x}Co_xO_{4-\delta}$ and (d–f) $Sm_{1.8}Ce_{0.2}Cu_{1-x}Co_xO_{4+\delta}$ at $x = 0$ (a and d), 0.2 (b and e), and 0.4 (c and f).

spectra of CeO_2 (oxidation state = 4+) and Ce_2O_3 (oxidation state = 3+) [35], we find that the Ce 3d spectra of the $Sm_{1.8}Ce_{0.2}Cu_{1-x}Co_xO_{4+\delta}$ catalysts are similar to that of CeO_2 but different from that of Ce_2O_3. This means that the Ce ions of $Sm_{1.8}Ce_{0.2}Cu_{1-x}Co_xO_{4+\delta}$ exist in an oxidation state of 4+. Similar results have been obtained by other authors [36–39] and us [40]. It should be pointed out that the cobalt ions in the $NdSrCu_{1-x}Co_xO_{4-\delta}$ and $Sm_{1.8}Ce_{0.2}Cu_{1-x}Co_xO_{4+\delta}$ catalysts show a Co $2p_{3/2}$ peak at ca. 780 eV without the sighting of satellite peaks at ca. 790 eV, corroborating the presence of only Co^{3+} in the two series of catalysts. Based on the fact that there is no change in the oxidation state of the Nd, Sr, Sm, and Co elements, it is reasonable to assume that with the doping of Co, only the B-site copper ions vary in oxidation state.

According to the work of Machida et al. [29] and ourselves [40], we assign the signal of Cu $2p_{3/2}$ at BE = ca. 932.0 eV to Cu^+ ions, that at BE = ca. 933 eV (with shake-up satellite features in the 940–945-eV range) to Cu^{2+} ions, and that at BE = ca. 934 eV to Cu^{3+} ions. The shake-up peaks are generally believed to be due to charge transfer from neighboring oxygen ligands to an empty d-state of Cu^{2+}. Fig. 4 shows the Cu $2p_{3/2}$ and O 1s XPS spectra of $NdSrCu_{1-x}Co_xO_{4-\delta}$. For $x = 0$, 0.2 and 0.4, there is a main peak at ca. 933 eV with shake-up satellites located in the BE range of 940–945 eV (Fig. 4(A)), indicating the presence of Cu^{2+} ions [28]. Signals at ca. 934 eV due to Cu^{3+} ions are also detected and the intensity decreases with a rise in x value, indicating a drop in Cu^{3+} concentration (Fig. 4(A)). As for the O 1s spectra (Fig. 4(B)), the signal at BE = ca. 529 eV is attributed to lattice oxygen ($O^{2-}_{lattice}$) and the one at BE = ca. 531 eV to adsorbed oxygen species (such as O^-, O_2^- or O_2^{2-}) [41–43]; with increasing x value, the signal intensity of $O^{2-}_{lattice}$ increases whereas that of oxygen adspecies decreases, demonstrating that the doping of Co to the cuprate lattice affects the amount of oxygen adspecies.

Shown in Fig. 5 are the Cu $2p_{3/2}$ and O 1s spectra of $Sm_{1.8}Ce_{0.2}Cu_{1-x}Co_xO_{4+\delta}$. From Fig. 5(A), one can realize that with an increase in x value from 0 to 0.4, there is a decrease in shake-up satellite intensity (the I_s/I_m value decreased from 0.25 to 0.20; I_s and I_m stands for the intensity of the satellite and main peak, respectively), implying that there is a decrease in the amount of Cu^{2+} ions [28,31]. The signal at BE = ca. 932 eV is due to Cu^+ ions, and the signal intensity increases with a rise in x value, indicating that Co doping induces the generation and stabilization of Cu^+ ions. In the O 1s spectra (Fig. 5(B)), there is a signal at BE = ca. 528 eV attributable to $O^{2-}_{lattice}$ and a signal at BE = 530–531 eV ascribable to extra (over-stoichiometric) oxygen species. The latter is a tentative assignment based on the fact that the BE is between that of $O^{2-}_{lattice}$ and that of adsorbed oxygen. With a rise in x value, there is a decline in $O^{2-}_{lattice}$ signal intensity but a rise in extra (over-stoichiometric) oxygen signal intensity.

3.3. O_2-TPD studies

The behaviors of oxygen desorption from oxygen nonstoichiometric ABO_3 or A_2BO_4 catalysts have been investigated by several

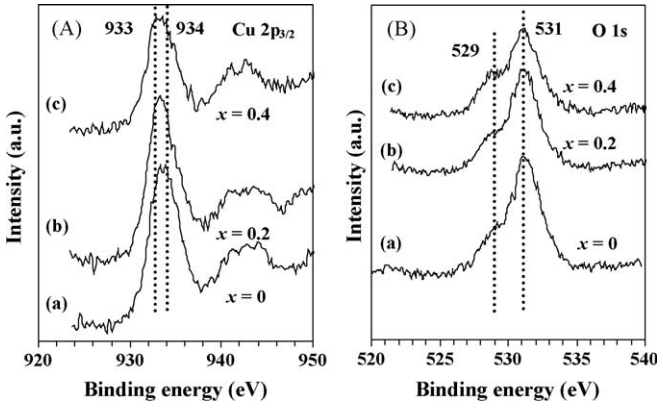

Fig. 4. (A) Cu $2p_{3/2}$ and (B) O 1s XPS spectra of $NdSrCu_{1-x}Co_xO_{4-\delta}$.

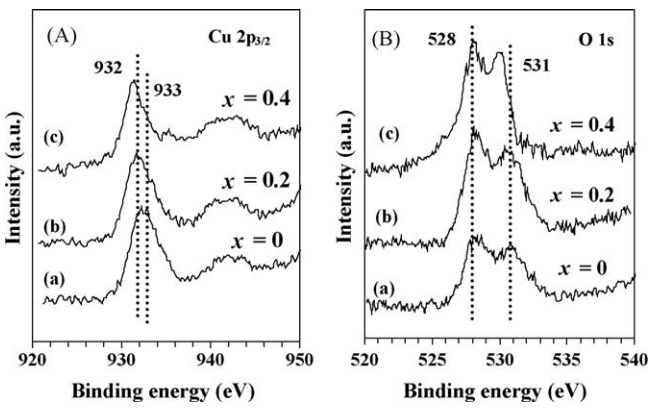

Fig. 5. (A) Cu $2p_{3/2}$ and (B) O 1s XPS spectra of $Sm_{1.8}Ce_{0.2}Cu_{1-x}Co_xO_{4+\delta}$.

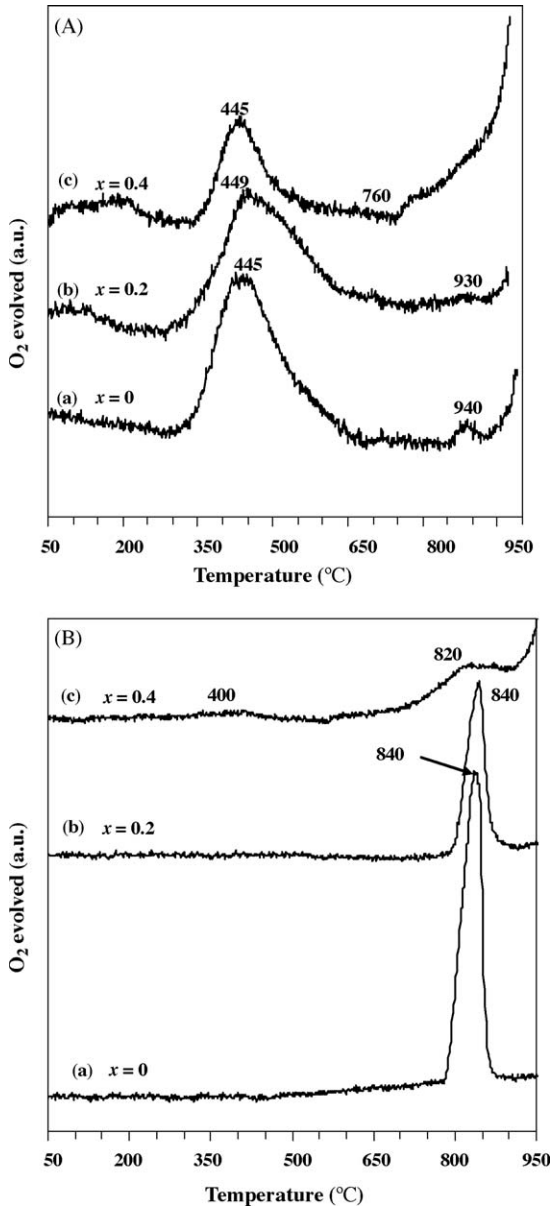

Fig. 6. O_2-TPD profiles of (A) $NdSrCu_{1-x}Co_xO_{4-\delta}$ and (B) $Sm_{1.8}Ce_{0.2}Cu_{1-x}Co_xO_{4+\delta}$.

research groups [13,17,19,42,44]. Shown in Fig. 6 are the O_2-TPD profiles of the $NdSrCu_{1-x}Co_xO_{4-\delta}$ and $Sm_{1.8}Ce_{0.2}Cu_{1-x}Co_xO_{4+\delta}$ catalysts. The spectra of the former show two peaks (Fig. 6(A)): that locates in the 300–700 °C range, and that starts from ca. 940, 930, and 760 °C for the samples with $x = 0$, 0.2, and 0.4, respectively. The amount of oxygen desorption in the 300–700 °C range is 61.0, 45.8, and 28.1 μmol/g_{cat} for the samples with $x = 0$, 0.2, and 0.4, respectively. Similar to the $La_{1-x}Sr_xCoO_{3-\delta}$ samples of reductive nonstoichiometric nature reported by Seiyama [17] and Yamazoe et al. [42], the peaks below 800 °C could be ascribed to α desorption originated from adsorbed oxygen at oxygen vacancies. Thus the amount of α desorption can be used to roughly estimate the amount of oxygen vacancies. Based on the amount of oxygen desorption in the 300–700 °C range, we deduce that the oxygen vacancy density of the $NdSrCu_{1-x}Co_xO_{4-\delta}$ catalysts decreases in the order of $NdSrCuO_{3.70} > NdSrCu_{0.8}Co_{0.2}O_{3.74} > NdSrCu_{0.6}Co_{0.4}O_{3.79}$. The desorption above 800 °C can be related to the removal of $O^{2-}{}_{lattice}$ that is accompanied by the partial reduction of Cu^{3+} to Cu^{2+}. In the case of the $Sm_{1.8}Ce_{0.2}Cu_{1-x}Co_xO_{4+\delta}$ catalysts (Fig. 6(B)), a phenomenon similar to that of oxygen excess perovskite-type oxides such as $La_{1-x}Sr_xMnO_{3+\delta}$ is observed [13,17]. The $Sm_{1.8}Ce_{0.2}CuO_{4.05}$ sample shows a very intense peak near 840 °C. For a Co substitution of $x = 0.2$, the peak at ca. 840 °C declines in intensity. At $x = 0.4$, the peak above 800 °C reduces to a small peak at ca. 820 °C and there is the appearance of a weak peak at ca. 400 °C. The amount of oxygen desorption corresponding to the weak signal at ca. 400 °C is 8.1 μmol/g_{cat}. The desorption peaks at low temperature are ascribed to α desorption and the ones above 800 °C to β desorption ascribable to the reduction of Cu^{2+} to Cu^{+}. The partial substitution of Co for Cu simply results in a decline in Cu^{2+} concentration and hence a decrease in the amount of cation vacancies without generating any oxygen vacancies. This is why at $x = 0.2$, α desorption is not significant. At $x = 0.4$, the extent of Co substitution becomes high enough to induce the generation of more over-stoichiometric oxygen and the peak corresponding to α desorption emerges.

3.4. H_2-TPR studies

The H_2-TPR profiles of $NdSrCu_{1-x}Co_xO_{4-\delta}$ and $Sm_{1.8}Ce_{0.2}Cu_{1-x}Co_xO_{4+\delta}$ are shown in Fig. 7. For the $NdSrCu_{1-x}Co_xO_{4-\delta}$

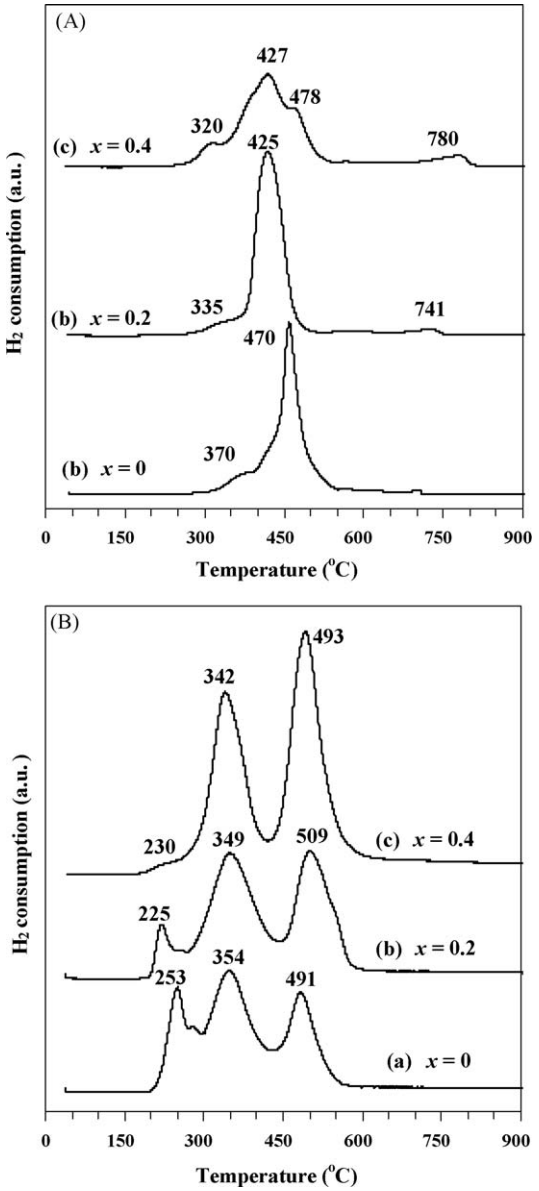

Fig. 7. H_2-TPR profiles of (A) $NdSrCu_{1-x}Co_xO_{4-\delta}$ and (B) $Sm_{1.8}Ce_{0.2}Cu_{1-x}Co_xO_{4+\delta}$.

samples (Fig. 7(A)), there are reduction bands at 370 and 470 °C for $x = 0$, corresponding to a total H_2 consumption of 2.96 mmol/g_{cat}; at 335, 425, and 741 °C for $x = 0.2$, corresponding to a total H_2 consumption of 3.16 mmol/g_{cat}; and at 320, 427, 478, and 780 °C for $x = 0.4$, corresponding to a total H_2 consumption of 3.54 mmol/g_{cat}. For the $Sm_{1.8}Ce_{0.2}Cu_{1-x}Co_xO_{4+\delta}$ samples (Fig. 7(B)), there are reduction bands detected at 253, 354, and 491 °C for $x = 0$; at 225, 349, and 509 °C for $x = 0.2$; and at 230, 342 and 493 °C for $x = 0.4$. The total H_2 consumption is 2.02, 2.24, and 2.50 mmol/g_{cat}, respectively. Apparently, the amount of H_2 consumption augments at elevated Co-doping level. This is understandable due to the presence of only Co^{3+} in the two series of catalysts. However, since the reduction of copper and cobalt ions in perovskites by H_2 takes place in similar temperature ranges [8,17,45,46], it is hard to clearly explain the ascription of the reduction bands in Fig. 7. Nevertheless, we find that the values of H_2 consumption are close to the corresponding theoretical values (3.39, 3.49 and 3.64 mmol/g_{cat} over $NdSrCu_{1-x}Co_xO_{4-\delta}$ and 2.21, 2.35 and 2.54 mmol/g_{cat} over $Sm_{1.8}Ce_{0.2}Cu_{1-x}Co_xO_{4+\delta}$ at $x = 0$, 0.2, and 0.4, respectively) estimated according to the bulk Cu^{3+}/Cu^{2+} or Cu^{2+}/Cu^{+} ratios (Table 1). That is to say, the reduction bands in Fig. 7 could be ascribed to the reduction of copper and/or cobalt ions from high to low-oxidation state (even to metallic state) [8,29,45,46].

3.5. Catalytic evaluation

In the blank experiment, the light-off temperature ($T_{50\%}$, methane conversion = 50%) and the temperature for complete combustion ($T_{100\%}$, methane conversion = 100%) are 840 and 870 °C over quartz sands (not shown here), respectively. This indicates that the homogeneous reaction of methane and oxygen below 700 °C was insignificant. Fig. 8 shows the activities of the $NdSrCu_{1-x}Co_xO_{4-\delta}$ and $Sm_{1.8}Ce_{0.2}Cu_{1-x}Co_xO_{4+\delta}$ catalysts for the total oxidation of methane under the conditions of methane/oxygen molar ratio = 1/20 and space velocity = 10,000 h^{-1}. Below 500 °C, methane conversion over these catalysts is not significant, while above 500 °C its conversion increases markedly. In the case of $NdSrCu_{1-x}Co_xO_{4-\delta}$ (Fig. 8(A)), the catalytic activity follows a sequence of $NdSrCuO_{3.70} > NdSrCu_{0.8}Co_{0.2}O_{3.74} > NdSrCu_{0.6}Co_{0.4}O_{3.79}$. The $T_{50\%}$ and $T_{100\%}$ values are ca. 550 and 610 °C over $NdSrCuO_{3.70}$, 570 and 630 °C over $NdSrCu_{0.8}Co_{0.2}O_{3.74}$, and 580 and 650 °C over $NdSrCu_{0.6}Co_{0.4}O_{3.79}$, respectively. For the $Sm_{1.8}Ce_{0.2}Cu_{1-x}Co_xO_{4+\delta}$ catalysts (Fig. 8(B)), the performance follows the order of $Sm_{1.8}Ce_{0.2}Cu_{0.6}Co_{0.4}O_{4.19} > Sm_{1.8}Ce_{0.2}Cu_{0.8}Co_{0.2}O_{4.10} > Sm_{1.8}Ce_{0.2}CuO_{4.05}$. The $T_{50\%}$ and $T_{100\%}$ are ca. 690 and 740 °C over $Sm_{1.8}Ce_{0.2}CuO_{4.05}$, 610 and 670 °C over $Sm_{1.8}Ce_{0.2}Cu_{0.8}Co_{0.2}O_{4.10}$, and 560 and 630 °C over $Sm_{1.8}Ce_{0.2}Cu_{0.6}Co_{0.4}O_{4.19}$, respectively. For the sake of making better comparison, methane consumption rates over the catalysts are shown in Fig. 8(C) and (D). It is found that the methane consumption rates (1.4–5.3 μmol/(g s)) over our catalysts at 500 °C are much higher than those (0.31–0.81 μmol/(g s)) over the $AFeO_3$ (A = La, Nd, Sm) and $LaFe_{1-x}Mg_xO_3$ ($x = 0$–0.5) catalysts [10]. Over the $LaCoO_3$ catalyst prepared by the sol–gel method, the $T_{50\%}$ and $T_{100\%}$ are ca. 560 and 635 °C (Fig. 8(A) and (B)), respectively, under the reaction conditions same as those over the $NdSrCu_{1-x}Co_xO_{4-\delta}$ and $Sm_{1.8}Ce_{0.2}Cu_{1-x}Co_xO_{4+\delta}$ catalysts. Apparently, the $LaCoO_3$ is inferior to $NdSrCuO_{3.70}$ in catalytic performance. From the above results, one can realize that our perovskite-like oxide catalysts perform well for the complete oxidation of methane. It is worth pointing out that the products detected are

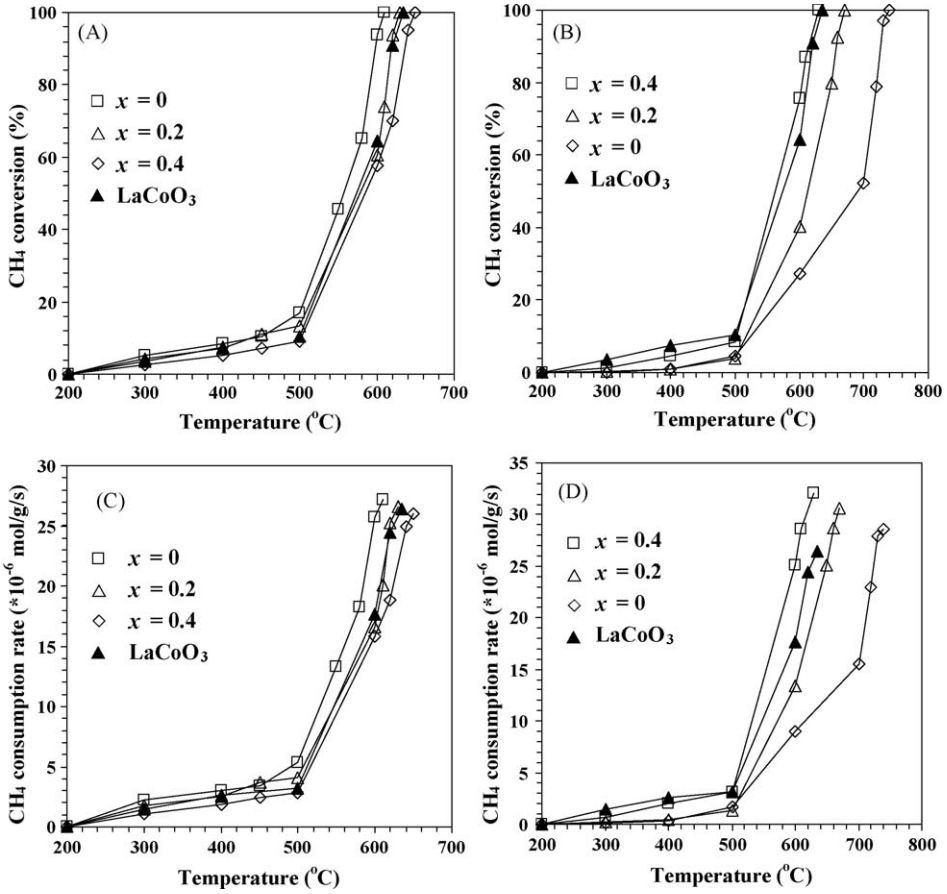

Fig. 8. CH_4 conversion (A and B) and CH_4 consumption rate (C and D) as a function of reaction temperature over (A and C) $NdSrCu_{1-x}Co_xO_{4-\delta}$ and (B and D) $Sm_{1.8}Ce_{0.2}Cu_{1-x}Co_xO_{4+\delta}$ as well as over $LaCoO_3$ under the conditions of CH_4/O_2 molar ratio = 1/20 and space velocity = 10,000 h^{-1}.

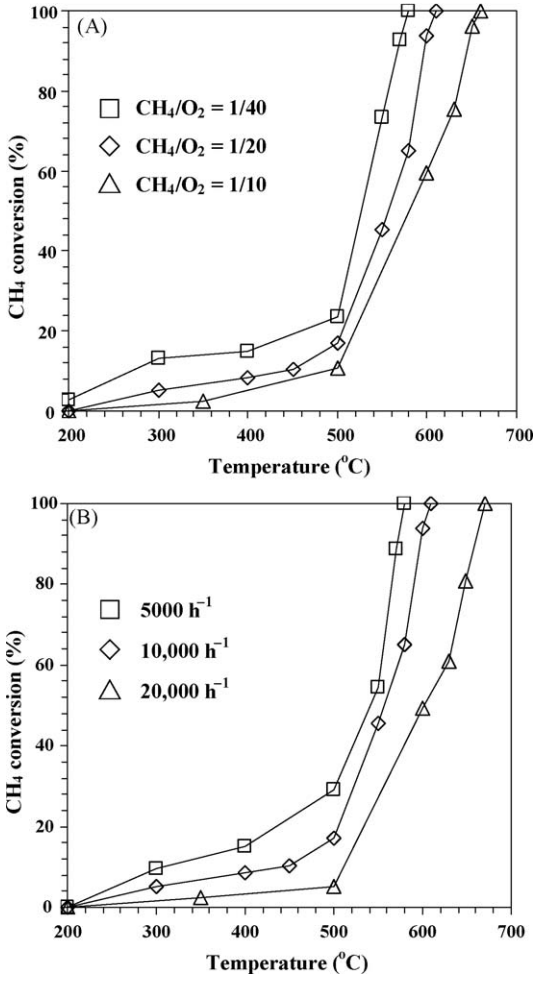

Fig. 9. Effects of (A) CH_4/O_2 molar ratio at space velocity = 10,000 h^{-1} and (B) space velocity at CH_4/O_2 molar ratio = 1/20 on the catalytic activity of $NdSrCuO_{3.70}$.

essentially CO_2 and H_2O, as confirmed by the estimated carbon balance of 99%.

Due to the best catalytic performance of the $NdSrCuO_{3.70}$ sample, we selected it to investigate the effects of methane/oxygen molar ratio and space velocity on the catalytic activity, and the results are shown in Fig. 9. As expected, there is significant augmentation in catalytic activity with increasing oxygen content in the reactant stream (Fig. 9(A)), and the catalytic activity decreases at elevated space velocities (Fig. 9(B)).

Assuming isothermal plug flow conditions and methane first order reaction rate expression (zero order for oxygen) and taking into account the activity data (Fig. 8), we obtained the Arrhenius plots, as shown in Fig. 10. The good linear relationship between ln k and reverse temperature suggests the exclusion of diffusion limitations. In other words, the oxidation of methane over the catalysts underwent in the kinetic region. The estimated apparent activation energy (E_a) was 73.7, 77.9, and 81.9 kJ/mol for $NdSrCu_{1-x}Co_xO_{4-\delta}$, and 79.5, 77.9, and 74.2 kJ/mol for $Sm_{1.8}Ce_{0.2}Cu_{1-x}Co_xO_{4+\delta}$ at $x = 0$, 0.2, and 0.4, respectively. The values (74–82 kJ/mol) of E_a for these catalysts are similar to those (77 kJ/mol) for the $Sm_{1-x}Sr_xMnO_3$ ($x = 0.3$, 0.5) samples [9], but lower than those (85–107 kJ/mol) for $LaMn_{1-x}Cu_xO_3$ ($x = 0$–0.6) and $LaCo_{1-x}Cu_xO_3$ ($x = 0$, 0.2, 1) [8], $AFeO_3$ (A = La, Nd, Sm) and $LaFe_{1-x}Mg_xO_3$ ($x = 0$–0.5) [10], $La_{1-x}A_xBO_3$ (A = Sr, Ce; B = Co, Mn) [18], and $LaCo_{1-x}Fe_xO_3$ [20]. These results reveal that methane can be activated more readily over our catalysts.

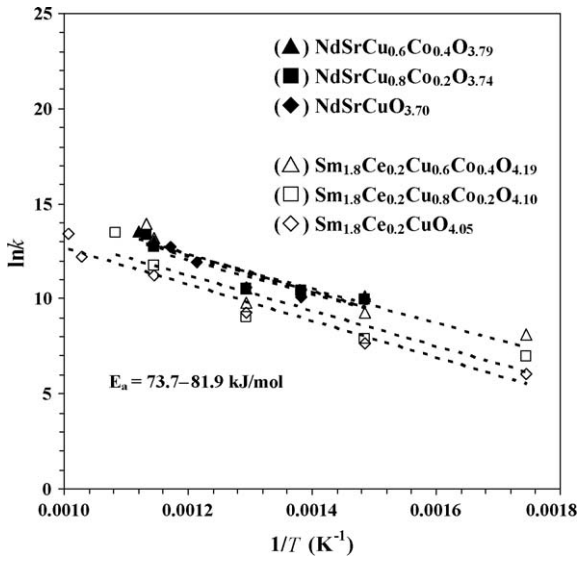

Fig. 10. Arrhenius plots for $NdSrCu_{1-x}Co_xO_{4-\delta}$ and $Sm_{1.8}Ce_{0.2}Cu_{1-x}Co_xO_{4+\delta}$ catalysts.

4. Discussion

4.1. Oxygen nonstoichiometry and catalytic performance

It is well known that $ABO_{3-\delta}$ show good catalytic performance for methane combustion. The $A_2BO_{4-\delta}$ are thermally more stable than $ABO_{3-\delta}$ and have been described as novel catalysts for hydrocarbons combustion [28–30]. It is generally accepted that the increases in oxygen vacancy concentration (δ) and B-site ion redox ability facilitate the combustion of methane [1–4,16,17]. Therefore, one can expect that a proper adjustment of the amount of oxygen vacancies and of the distribution of B-site ions oxidation states would generate a perovskite-related material with optimal catalytic performance.

As revealed in the XRD investigations, the $NdSrCu_{1-x}Co_xO_{4-\delta}$ and $Sm_{1.8}Ce_{0.2}Cu_{1-x}Co_xO_{4+\delta}$ samples are single-phase and tetragonal in structure with (T structure) and without (T' structure) apical oxygen atoms, respectively. An important structural difference between the T and T' structure (Fig. 2) is that in the former, the Cu atom is located at the center of a CuO_6 octahedron and the Nd or Sr atoms are in ninefold coordination, whereas in the latter, the Cu atom is in a square CuO_4 unit and the Sm or Ce atoms are in nearly cubic eightfold coordination. It is envisioned that the doping of Co ions would regulate the oxidation state of Cu (or even that of Co itself) and oxygen vacancy density without having the backbone structure affected. Our results show that the doping with Co ions caused no structural destruction on $NdSrCuO_{4-\delta}$. Due to the mismatch of bond length between the lanthanide bilayers and the copper–oxygen layers, it is possible to have transition from tetragonal to cubic phase. When the amount of doped Co increased to a higher level ($x > 0.6$), such a phenomenon became significant (XRD results of the samples with $x > 0.6$ are not shown in this paper). The results reported by Lappas and Prassides [47] demonstrated that the Jahn-Teller distortion of the octahedra was strongly reduced due to the substitution of Co by Cu ions.

Previous work of Gao and Au suggested that Nd_2CuO_4 is tetragonal (T') [48]. Goodenough et al. illustrated that there is a sequence of $|CuO_2|Nd–O_2–Nd|CuO_2|$, i.e. fluorite layer and CuO_2 sheet, in this structure [39,44]. It has been pointed out that in order to retain electroneutrality, the substitution of Nd^{3+} with Ba^{2+} would result in the formation of oxygen vacancies or the oxidation of Cu^{2+}, whereas the substitution of Nd^{3+} with Ce^{4+} would lead to

the presence of extra (over-stoichiometric) oxygen or the reduction of Cu^{2+}. The oxygen vacancies or the extra oxygen can exist in the CuO_2 sheet in the form of $|CuO_{2-x}|Nd–O_2–Nd|CuO_{2-x}|$ or $|CuO_{2+x}|Nd–O_2–Nd|CuO_{2+x}|$, respectively. The oxygen vacancies and the interstitial oxygen can be present in the fluorite layer as $|CuO_2|Nd–O_{2-x}–Nd|CuO_2|$ and $|CuO_2|Nd–O_{2+x}–Nd|CuO_2|$, respectively. The CuO_2 sheet is responsible for the redox action. The nature of the $NdSrCu_{1-x}Co_xO_{4-\delta}$ and $Sm_{1.8}Ce_{0.2}Cu_{1-x}Co_xO_{4+\delta}$ catalysts can be illustrated in a similar manner. For the balance of charge, the substitution of Nd^{3+} with Sr^{2+} would give rise to the formation of oxygen vacancies or the oxidation of Cu^{2+} (to Cu^{3+}), whereas the substitution of Sm^{3+} with Ce^{4+} would lead to the presence of extra oxygen or the reduction of Cu^{2+} (to Cu^{+}).

From the O 1s spectra (Figs. 4(B) and 5(B)), one can deduce that there are oxygen species on the surface: (a) $O^{2-}{}_{lattice}$ at BE = 528 eV; (b) extra oxygen ($O^{2-}{}_{extra}$) at BE = 530–531 eV, and (c) adsorbed oxygen (O^-, O_2^- or O_2^{2-}) at BE = 531 eV. That is to say, in addition to $O^{2-}{}_{lattice}$, there are adsorbed oxygen species on $NdSrCu_{1-x}Co_xO_{4-\delta}$ whereas on $Sm_{1.8}Ce_{0.2}Cu_{1-x}Co_xO_{4+\delta}$ over-stoichiometric oxygen species are present. From Table 1, one can observe that the doping of Co ions causes the δ value of $NdSrCu_{1-x}Co_xO_{4-\delta}$ to decrease and that of $Sm_{1.8}Ce_{0.2}Cu_{1-x}Co_xO_{4+\delta}$ to increase. In other words, the addition of Co ions induces adjustment in oxygen vacancies or oxygen extra content as well as adjustment in Cu ion valence. Rao [49] pointed out that the O^- species located at the oxygen vacancies of the Sr-doped catalysts caused a rise of Cu^{3+} concentration. For the $Sm_{1.8}Ce_{0.2}Cu_{1-x}Co_xO_{4+\delta}$ catalysts, it is extra oxygen rather than oxygen vacancies that has been found. It has been reported that there are O^- species in oxygen-excess structure such as $La_2CuO_{4+\delta}$ [50] which can be described as $La_2(Cu^{2+}{}_{1-x}Cu^{3+}{}_x)O_4{}^{2-}(O^-)_\delta$. The redox ($Cu^{3+} + O^{2-} \Leftrightarrow Cu^{2+} + O^-$) of O^{2-}/O^- and Cu^{3+}/Cu^{2+} in La_2CuO_4 have been proposed by Grenier et al. [51] and Magnone et al. [52]. The above results suggest that the O^{2-}/O^- redox could occur in both cases of oxygen vacancies and extra oxygen. It is believed that the O^- species on the catalysts are active for the catalytic combustion of hydrocarbons [53]. By comparing the XPS data of $Sm_{1.8}Ce_{0.2}Cu_{1-x}Co_xO_{4+\delta}$ and $NdSrCu_{1-x}Co_xO_{4-\delta}$, one can notice that the latter contains a larger amount of adsorbed oxygen. Among the catalysts, $NdSrCuO_{3.70}$ shows the richest amount of oxygen vacancies and subsequently the highest amount of adsorbed oxygen. Hence, it exhibits the best catalytic activity.

It was proposed by Voorhoeve et al. [54] that oxidation reactions on ABO_3 catalysts can be classified into two types: intrafacial reactions and suprafacial reactions. The latter are believed to proceed at relatively low temperatures while the former are operative at high temperatures. Based on the available data and information, methane catalytic combustion at low temperatures over the ABO_3 catalysts is a suprafacial reaction involving oxygen coming from the gas phase or locating at the oxygen vacancies of the catalysts. At high temperatures, methane reacts with the oxygen coming from the bulk of the catalyst following the intrafacial mechanism [2–4,17,53]. Furthermore, several authors demonstrated that (i) methane interacts with the oxygen on the catalyst surface, (ii) an oxygen-exchange reaction occurs prior to increase of catalytic activity, and (iii) the activation of O_2 is easier than the activation of methane C–H bonds [3,4]. It is believed that oxygen vacancies in the catalysts promote the adsorption and dissociation of oxygen molecules [3,4,18]. The extent of oxygen desorption reflects the amount of O_2 adsorbed on the active sites of the catalysts, which are related to the activity of catalytic reaction. Based on the results of O_2-TPD experiments (Section 3.3), one can estimate the amount of oxygen adspecies at the surface oxygen vacancies. The amount of active sites (oxygen vacancies or extra oxygen) of the catalysts, as reflected by the amount of O_2 desorption in the low-temperature range (Fig. 6), follows the sequence of $NdSrCuO_{3.70} > NdSrCu_{0.8}Co_{0.2}O_{3.74} > NdSrCu_{0.6}Co_{0.4}O_{3.79}$ or that of $Sm_{1.8}Ce_{0.2}Cu_{0.6}Co_{0.4}O_{4.19} > Sm_{1.8}Ce_{0.2}Cu_{0.8}Co_{0.2}O_{4.10} > Sm_{1.8}Ce_{0.2}CuO_{4.05}$. As aforementioned, the oxygen vacancies play an important role in oxidation reactions since they are responsible for the adsorption of gas-phase O_2 and they facilitate the diffusion of lattice oxygen from the bulk to the surface. Thus it is understandable that the order of decreasing catalytic performance follows the sequence of decreasing oxygen vacancy (or extra oxygen) density: $NdSrCuO_{3.70} > NdSrCu_{0.8}Co_{0.2}O_{3.74} > NdSrCu_{0.6}Co_{0.4}O_{3.79}$ and $Sm_{1.8}Ce_{0.2}Cu_{0.6}Co_{0.4}O_{4.19} > Sm_{1.8}Ce_{0.2}Cu_{0.8}Co_{0.2}O_{4.10} > Sm_{1.8}Ce_{0.2}CuO_{4.05}$.

The relationship between activity and bulk oxygen mobility for the methane oxidation reaction has been discussed before. The oxygen mobility can be related to the reducibility of the transition metal ions [20,24]. As revealed in Fig. 6, the onset temperatures of β oxygen desorption peaks decrease with the rise of Co-substitution level. One can deduce that the doping of Co into the $NdSrCuO_{4-\delta}$ and $Sm_{1.8}Ce_{0.2}CuO_{4+\delta}$ lattices results in enhancement of $O^{2-}{}_{lattice}$ mobility. It is noteworthy that the onset temperature of β oxygen desorption over the $Sm_{1.8}Ce_{0.2}Cu_{0.6}Co_{0.4}O_{4.19}$ catalyst is much lower than that over the $NdSrCu_{0.8}Co_{0.2}O_{3.74}$ and $NdSrCu_{0.6}Co_{0.4}O_{3.79}$ catalysts. By comparing the temperature for maximum reduction in the low-temperature range (Fig. 7), one can see that the $Sm_{1.8}Ce_{0.2}Cu_{0.6}Co_{0.4}O_{4.19}$ catalyst is much more easily reduced than the $NdSrCu_{0.8}Co_{0.2}O_{3.74}$ and $NdSrCu_{0.6}Co_{0.4}O_{3.79}$ catalysts. The results indicated that at high temperatures the $O^{2-}{}_{lattice}$ in the bulk of $Sm_{1.8}Ce_{0.2}Cu_{0.6}Co_{0.4}O_{4.19}$ is much more mobile than that in the bulk of the $NdSrCu_{0.8}Co_{0.2}O_{3.74}$ and $NdSrCu_{0.6}Co_{0.4}O_{3.79}$ catalysts. In other words, the diffusion of $O^{2-}{}_{lattice}$ from bulk to surface of $Sm_{1.8}Ce_{0.2}Cu_{0.6}Co_{0.4}O_{4.19}$ becomes facile at high temperatures. As demonstrated by Ferri and Forni [4] and Fierro [55], the rate of methane oxidation boosts when bulk oxygen becomes available since methane reacts with the oxygen coming from the bulk at high temperatures via the intrafacial mechanism. This may explain that despite the $NdSrCu_{0.8}Co_{0.2}O_{3.74}$ or $NdSrCu_{0.6}Co_{0.4}O_{3.79}$ catalyst is enriched with oxygen vacancies, the catalytic performance is similar or even inferior to that of the $Sm_{1.8}Ce_{0.2}Cu_{0.6}Co_{0.4}O_{4.19}$ catalyst. The discrepancy in catalytic performance of these materials can be also explained according to the E_a values. With a rise in Co-substitution level, the E_a value increases for the Sr-doped catalysts, whereas it decreases for the Ce-doped ones, coinciding with the change trend in catalytic activity of each serial catalysts.

It is known that the oxidation of hydrocarbons over ABO_3 catalysts involving adsorbed oxygen depends greatly on the partial pressure of oxygen in the reactant feed [17]. The higher the O_2 partial pressure and the longer the contact time (i.e. the lower the space velocity), the more the amount of the oxygen adspecies formed at the oxygen vacancies, and hence the more favorable the oxidation of methane. This is confirmed by the results obtained at various methane/oxygen molar ratios and space velocities (Fig. 9).

4.2. Cu ion couples and catalytic performance

The Nd, Sr and Sm in ABO_3 or A_2BO_4 compounds are usually in 3+, 2+ and 3+ states, respectively. Based on the results of lattice parameters, Huang et al. [38] and Goodenough [39] pointed out that the valence of Ce in $Nd_{2-x}Ce_xCuO_{4-\delta}$ is not trivalent but tetravalent. On the other hand, based on the XPS results, Hor et al. [37] concluded that the cerium in $Nd_{2-x}Ce_xCuO_{4-\delta}$ existed as Ce^{4+}. In the present study, the Ce 3d spectra of the $Sm_{1.8}Ce_{0.2}Cu_{1-x}Co_xO_{4+\delta}$ catalysts also indicated that the Ce ions are tetravalent. Our XPS results proved that the Co ions in $NdSrCu_{1-x}Co_xO_{4-\delta}$ and $Sm_{1.8}Ce_{0.2}Cu_{1-x}Co_xO_{4+\delta}$ are trivalent due to the extremely easy oxidation of Co^{2+} to Co^{3+} during the calcination process. It has been established that the incorporation

of excess oxygen in the $La_2CoO_{4+\delta}$ system occurs readily, especially when the calcination process undergoes in air [56,57].

It is commonly believed that copper exists as Cu^{3+} and Cu^{2+} in $La_{2-x}Sr_xCuO_{4-\delta}$ [27,33,58]. Nevertheless, there is claim that copper exists solely as Cu^{2+} [59]. Based on the results of XPS investigation over $Nd_{2-x}Ce_xCuO_{4+\delta}$, Suzuki et al. [36] and Liang et al. [59] reported the generation of Cu^+ as a result of Ce^{4+} substitution. The results of chemical analysis (Table 1) and XPS studies (Figs. 4(A) and 5(A)) show that besides Cu^{2+}, there are Cu^{3+} ions in $NdSrCu_{1-x}Co_xO_{4-\delta}$; and besides Cu^{2+} ions, there are Cu^+ ions in $Sm_{1.8}Ce_{0.2}Cu_{1-x}Co_xO_{4+\delta}$. Since the BE of the 2p electrons of Cu^{3+} ions should be higher than that of Cu^{2+} or Cu^+ ions, a peak at higher BE is expected for Cu^{3+}, as can be seen in the XPS spectra of Cu $2p_{3/2}$ (Fig. 4(A)).

The mechanism of C_3H_8 oxidation over $La_{2-x}Sr_xCo^{2+}{}_{1-y}Co^{3+}{}_yO_4$ as illustrated by Luo et al. involves Co^{3+} as the active center. With C_3H_6 adsorbed on Co^{3+}, the reaction between C_3H_6 and $O^{2-}{}_{lattice}$ took place and the consumed $O^{2-}{}_{lattice}$ was replenished by O_2 from the gas phase [30]. The mechanism of methane oxidation over $LaSrCo^{3+}{}_{1-x}Co^{4+}{}_xO_4$ as proposed by Borovskikh et al. [24] involves (i) adsorption of methane and O_2 on the catalyst surface; (ii) O^{2-} from the bulk reduces Co^{4+} to Co^{3+} and the generated active oxygen oxidizes CH_4; and (iii) the surface oxygen species oxidize Co^{3+} to Co^{4+} and/or become $O^{2-}{}_{lattice}$ after incorporation into the bulk. For the methane oxidation reaction, the rate-limiting step is assumed to be the breaking of the first C–H bond and the formation of a hydroxyl group [60]. On the basis of the results of previous work [23,24,30,60], the possible reaction steps are

$$O_2\ (gas) \rightarrow O_2\ (adsorbed) \rightarrow 2[O]\ (adsorbed)$$

$$H_3C{-}H + [O][CuO_x] \rightarrow [H_3C^\bullet] + [OH][CuO_x]$$

$$[H_3C^\bullet] + [CuO_x] \rightarrow [CuO_yCO_2] + H_2O$$

$$[CuO_yCO_2] \rightarrow [CuO_y] + CO_2$$

$$[CuO_y] + O_2 \rightarrow [O][CuO_x]$$

$$[OH][CuO_x] + [OH][CuO_x] \rightarrow 2[CuO_x] + H_2O + [O]$$

The presence of active sites $[CuO_x]$ appears to be essential for the fast and complete oxidation of methane. Similar to $La_{2-x}Sr_x-Co^{2+}{}_{1-y}Co^{3+}{}_yO_4$ reported by Yang et al. [30], one can reasonably deduce that $[Cu^{3+}O_x]$ might be the active center in the case of the $NdSrCu_{1-x}Co_xO_{4-\delta}$ catalysts. The higher the Cu^{3+} concentration in $NdSrCu_{1-x}Co_xO_{4-\delta}$, the larger would be the amount of activated (by adsorbed oxygen species) methane at the active sites $[CuO_x]$, and therefore the better the catalytic performance. Since the content of Cu^{3+} in $NdSrCu_{1-x}Co_xO_{4-\delta}$ decreases with a rise in Co-doping level (Table 1), the catalysts decrease in activity in the order of $NdSrCuO_{3.70} > NdSrCu_{0.8}Co_{0.2}O_{3.74} > NdSrCu_{0.6}Co_{0.4}O_{3.79}$ (Fig. 8(A) and (C)). Zhu et al. pointed out that the redox action of copper ions with $O^{2-}{}_{lattice}$ in $La_{2-x}A'_xCuO_4$ (A′ = Sr, Th) plays an important role in enhancing catalytic performance [31,33]. We expect that similar scenario would occur in the $NdSrCu_{1-x}Co_xO_{4-\delta}$ and $Sm_{1.8}Ce_{0.2}Cu_{1-x}Co_xO_{4+\delta}$ catalysts. The catalytic activities could be related to the redox processes: $Cu^{3+} \Leftrightarrow Cu^{2+}$ in the $NdSrCu_{1-x}Co_xO_{4-\delta}$ and $Cu^{2+} \Leftrightarrow Cu^+$ in the $Sm_{1.8}Ce_{0.2}Cu_{1-x}Co_xO_{4+\delta}$ catalysts. Due to the fact that Cu^{2+} (d^9 configuration) is more stable than Cu^{3+} (d^8 configuration) or Cu^+, the higher the Cu^{3+} or Cu^+ concentration, the easier would be the redox processes [27,33]. The enhancement of Cu^{3+}/Cu^{2+} redox ability improves the catalytic performance as confirmed in the case of the $NdSrCu_{1-x}Co_xO_{4-\delta}$ catalysts. Thus it is understandable that for the $Sm_{1.8}Ce_{0.2}-Cu_{1-x}Co_xO_{4+\delta}$ samples (Fig. 8(B) and (D)), the activity follows the order of $Sm_{1.8}Ce_{0.2}Cu_{0.6}Co_{0.4}O_{4.19} > Sm_{1.8}Ce_{0.2}Cu_{0.8}Co_{0.2}O_{4.10} > Sm_{1.8}Ce_{0.2}CuO_{4.05}$, in agreement with the declining concentration of Cu^+ ions (Table 1).

5. Conclusion

Single-phase $NdSrCu_{1-x}Co_xO_{4-\delta}$ of *T* structure and $Sm_{1.8}Ce_{0.2}-Cu_{1-x}Co_xO_{4+\delta}$ (x = 0–0.4) of *T′* structure were prepared via the citric acid complexing method that coupled with ultrasonic treatment. The catalysts possess BET surface areas of 4–8 m^2/g. The $NdSrCu_{1-x}Co_xO_{4-\delta}$ catalysts are of reductive nonstoichiometry while the $Sm_{1.8}Ce_{0.2}Cu_{1-x}Co_xO_{4+\delta}$ catalysts are of oxidative nonstoichiometry. With a rise in Co-doping level, the oxygen vacancy density of $NdSrCu_{1-x}Co_xO_{4-\delta}$ decreases whereas the extra (over-stoichiometric) oxygen amount of $Sm_{1.8}Ce_{0.2}Cu_{1-x}Co_xO_{4+\delta}$ increases. There are Cu^{3+}/Cu^{2+} in $NdSrCu_{1-x}Co_xO_{4-\delta}$ and Cu^{2+}/Cu^+ in $Sm_{1.8}Ce_{0.2}Cu_{1-x}Co_xO_{4+\delta}$. Under the conditions of methane/oxygen = 1/20 and space velocity = 10,000 h^{-1}, the catalytic activity of $NdSrCu_{1-x}Co_xO_{4-\delta}$ follows a decreasing order of $NdSrCuO_{3.70} > NdSrCu_{0.8}Co_{0.2}O_{3.74} > NdSrCu_{0.6}Co_{0.4}O_{3.79}$, whereas that of $Sm_{1.8}Ce_{0.2}Cu_{1-x}Co_xO_{4+\delta}$ shows a decreasing order of $Sm_{1.8}Ce_{0.2}Cu_{0.6}Co_{0.4}O_{4.19} > Sm_{1.8}Ce_{0.2}Cu_{0.8}Co_{0.2}O_{4.10} > Sm_{1.8}Ce_{0.2}-CuO_{4.05}$. The catalytic performance is in concord with the sequence of decreasing oxygen nonstoichiometry and Cu^{3+} concentration or oxygen excess density and Cu^+ concentration. Based on the results, we conclude that the high-oxygen nonstoichiometry and the strong Cu^{3+}/Cu^{2+} or Cu^{2+}/Cu^+ redox ability account for the good activity observed in the combustion of methane over the catalysts.

Acknowledgements

This work was supported by the Natural Science Foundation of Beijing Municipality (Key Class B project of grant number KZ200610005004) and Funding Project for Academic Human Resources Development in Institutions of Higher Learning under the Jurisdiction of Beijing Municipality (PHR (IHLB)). CTA thanks the RGC, Hong Kong Special Administration Region for financial support (Grant HKBU 200106).

References

[1] T.V. Choudhary, S. Banerjee, V.R. Choudhary, Appl. Catal. A 234 (2002) 1–23.
[2] M.A. Peña, J.L.G. Fierro, Chem. Rev. 101 (2001) 1981–2018.
[3] L. Marchetti, L. Forni, Appl. Catal. B 15 (1998) 179–187.
[4] D. Ferri, L. Forni, Appl. Catal. B 16 (1998) 119–126.
[5] R. Leanza, I. Rossetti, L. Fabbrini, C. Oliva, L. Forni, Appl. Catal. B 28 (2000) 55–64.
[6] I. Rossetti, L. Forni, Appl. Catal. B 33 (2001) 345–352.
[7] E. Campagnoli, A.C. Tavares, L. Fabbrini, I. Rossetti, Yu.A. Dubitsky, A. Zaopo, L. Forni, J. Mater. Sci. 41 (2006) 4713–4719.
[8] L. Lisi, G. Bagnasco, P. Ciambelli, S. De Rossi, P. Porta, G. Russo, M. Turco, J. Solid State Chem. 146 (1999) 176–183.
[9] P. Ciambelli, S. Cimino, S. De Rossi, M. Faticanti, L. Lisi, G. Minelli, I. Pettiti, P. Porta, G. Russo, M. Turco, Appl. Catal. B 24 (2000) 243–253.
[10] P. Ciambelli, S. Cimino, S. De Rossi, L. Lisi, G. Minelli, P. Porta, G. Russo, Appl. Catal. B 29 (2001) 239–250.
[11] P. Ciambelli, S. Cimino, L. Lisi, M. Faticanti, G. Minelli, I. Pettiti, P. Porta, Appl. Catal. B 33 (2001) 193–203.
[12] S. Cimino, L. Lisi, S. De Rossi, M. Faticanti, P. Porta, Appl. Catal. B 43 (2003) 397–406.
[13] S. Ponce, M.A. Peña, J.L.G. Fierro, Appl. Catal. B 24 (2000) 193–205.
[14] R.M. García de la Cruz, H. Falcón, M.A. Peña, J.L.G. Fierro, Appl. Catal. B 33 (2001) 45–55.
[15] H. Falcón, J.A. Barbero, G. Araujo, M.T. Casais, M.J. Martínez-Lope, J.A. Alonso, J.L.G. Fierro, Appl. Catal. B 53 (2004) 37–45.
[16] H. Arai, T. Yamada, K. Eguchi, T. Seiyama, Appl. Catal. 26 (1986) 265–276.
[17] T. Seiyama, in: L.G. Tejuca, J.L.G. Fierro (Eds.), Properties and Applications of Perovskite-type Oxides, Marcel Dekker, New York, 1993, pp. 215–234.
[18] S. Royer, H. Alamdari, D. Duprez, S. Kaliaguine, Appl. Catal. B 58 (2005) 273–288.
[19] M. Alifanti, R. Auer, J. Kirchnerova, F. Thyrion, P. Grange, B. Delmon, Appl. Catal. B 41 (2003) 71–81.
[20] S. Royer, D. Duprez, S. Kaliaguine, J. Catal. 234 (2005) 364–375.
[21] S. Royer, A. Van Neste, R. Davidson, S. McIntyre, S. Kaliaguine, Ind. Eng. Chem. Res. 43 (2004) 5670–5680.
[22] H. Zhang, Y. Shimizu, Y. Teraoka, N. Miura, N. Yamazoe, J. Catal. 121 (1990) 432–440.

[23] M. Alifanti, J. Kirchnerova, B. Delmon, D. Klvana, Appl. Catal. A 262 (2004) 167–176.
[24] L. Borovskikh, G. Mazo, E. Kemnitz, Solid State Sci. 5 (2003) 409–417.
[25] C. Oliva, S. Cappelli, A. Kryukov, G.L. Chiarello, A.V. Vishniakov, L. Forni, J. Mol. Catal. A 247 (2006) 248–252.
[26] L. Fabbrini, I. Rossetti, L. Forni, Appl. Catal. B 63 (2006) 131–136.
[27] N. Mizuno, M. Yamato, M. Tanaka, M. Misono, Chem. Mater. 1 (1989) 232–236.
[28] N. Guilhaume, S.D. Peter, M. Primet, Appl. Catal. B 10 (1996) 325–344.
[29] M. Machida, K. Ochiai, K. Ito, K. Ikeue, J. Catal. 238 (2006) 58–66.
[30] X. Yang, L. Luo, H. Zhong, Appl. Catal. A 272 (2004) 299–303.
[31] J. Zhu, Z. Zhao, D. Xiao, J. Li, X. Yang, Y. Wu, Catal. Commun. 7 (2006) 29–32.
[32] J. Liu, Z. Zhao, C. Xu, A. Duan, Appl. Catal. B 78 (2007) 61–72.
[33] J. Zhu, Z. Zhao, D. Xiao, J. Li, X. Yang, Y. Wu, J. Mol. Catal. A 238 (2005) 35–40.
[34] M.W. Shafer, T. Penney, B.L. Olson, Phys. Rev. B 36 (1987) 4047–4050.
[35] L.Z. Gao, C.T. Au, Catal. Lett. 65 (2000) 91–98.
[36] T. Suzuki, M. Nagoshi, Y. Fukuda, K. Oh-Ishi, Y. Shono, M. Tachiki, Phys. Rev. B 42 (1990) 4263–4271.
[37] P.H. Hor, Y.Y. Xue, Y.Y. Sun, Y.C. Tao, Z.J. Huang, W. Rabalais, C.W. Chu, Physica C 159 (1989) 629–633.
[38] T.C. Huang, E. Moran, A.I. Nazzal, J.B. Torrance, Physica C 158 (1989) 148–152.
[39] J.B. Goodenough, Supercond. Sci. Technol. 3 (1990) 26–37.
[40] H.X. Dai, C.F. Ng, C.T. Au, J. Catal. 197 (2001) 251–266.
[41] G.U. Kulkarni, C.N.R. Rao, M.W. Roberts, J. Phys. Chem. 99 (1995) 3310–3316.
[42] N. Yamazoe, Y. Teraoka, T. Seiyama, Chem. Lett. 10 (1981) 1767–1770.
[43] J.L.G. Fierro, L.G. Tejuca, Appl. Surf. Sci. 27 (1987) 453–457.
[44] J.B. Goodenough, A. Manthiram, J. Solid State Chem. 88 (1990) 115–139.
[45] N. Tien-Thao, M.H. Zahedi-Niaki, H. Alamdari, S. Kaliaguine, J. Catal. 245 (2007) 348–357.
[46] R.D. Zhang, A. Villanueva, S. Alamdari, Kaliaguine, Appl. Catal. B 64 (2006) 220–233.
[47] A. Lappas, K. Prassides, J. Solid State Chem. 108 (1994) 59–67.
[48] L.Z. Gao, C.T. Au, J. Mol. Catal. A 168 (2001) 173–186.
[49] C.N.R. Rao, in: C.N.R. Rao (Ed.), Chemistry of Oxide Superconductors, Blackwell, Oxford, 1988, pp. 1–31.
[50] N. Casan-Pastor, P. Gomez-Romero, A. Fuetes, J.M. Navarro, M.J. Sanchis, S. Ondono, Physica C 216 (1993) 478–490.
[51] J.C. Grenier, A. Wattiaux, J.P. Doumerc, P. Dordor, L. Fournes, J.P. Chaminade, M. Pouchard, J. Solid State Chem. 96 (1992) 20–30.
[52] E. Magnone, G. Cerisola, M. Ferretti, A. Barbucci, J. Solid State Chem. 144 (1999) 8–15.
[53] A. Bielański, J. Haber, Oxygen in Catalysis, Dekker, New York, 1991, pp. 423–441.
[54] R.J.H. Voorhoeve, J.P. Remeika, P.E. Freeland, B.T. Mathias, Science 177 (1972) 353–354.
[55] J.L.G. Fierro, Catal. Today 8 (1990) 153–174.
[56] U. Lehmann, H.K. Müller-Buschbaum, Z. Anorg. Allg. Chem. 470 (1980) 59–63.
[57] R.A. Mohan Ram, P. Ganguly, C.N.R. Rao, Mater. Res. Bull. 23 (1988) 501–506.
[58] S. Rajadurai, J.J. Carberry, B. Li, C.B. Alcock, J. Catal. 131 (1991) 582–589.
[59] G. Liang, J. Chen, M. Croft, K.V. Ramanujachary, M. Greenblatt, M. Hedge, Phys. Rev. B 40 (1989) 2646–2649.
[60] A. Tschöpe, W. Liu, M. Flyzani-Stephanopoulos, J.Y. Ying, J. Catal. 157 (1995) 42–50.